Achiral plasmonic antennas enhance differential absorption to increase preferential detection of chiral single molecules

Saaj Chattopadhyay[1] and Julie S. Biteen[1,2,*]

[1] Applied Physics Program, University of Michigan, Ann Arbor, MI 48104 USA

[2] Department of Chemistry, University of Michigan, Ann Arbor, MI 48104 USA

* Correspondence to: jsbiteen@umich.edu

Abstract

Plasmonic antennas increase the photon flux in their vicinity, which can lead to plasmon-enhanced fluorescence for molecules near these nanostructures. Here, we combine plasmon-coupled fluorescence and fluorescence-detected circular dichroism to build a specific and sensitive detection strategy for chiral single molecules. Electromagnetic simulations indicate that a two-dimensional gold nanoparticle dimer antenna enhances the electric field and optical chirality of a plane wave in its near field. Furthermore, this optical chirality enhancement can be tuned based on the polarization of the incident electric field, such that enhancing the optical chirality via these antennas will increase the differential absorption of parity-inverted fields. We measured the fluorescence from single molecules of chiral absorbers—Cy5 J-dimers assembled in double-stranded DNA backbones—and achieved increased detectability of these right-handed molecules near achiral Au NP dimer antennas under right circularly polarized illumination. This strategy offers a new approach to distinguishing weakly fluorescent enantiomers.

Introduction

Molecular chirality is ubiquitous in biology, and this property affects interactions between molecules to dictate chemical and biological function. The molecular chirality can be determined by the interaction of a molecule with polarized light. While circular dichroism and optical rotatory dispersion have been used for over a century to study the concentration of optically active substances like sugars, these techniques require minimum concentrations ($\gtrsim$ 1 mM) and volumes ($\gtrsim$ 1 mL). The differential absorption from a single molecule is very low because of the mismatch of the size of molecules and the 400 – 700 nm wavelength of visible light. To build a probe for molecular chirality, the differential absorption must be enhanced in these molecules. Thus, recent work has focused on increasing both the detection capability and the differential signal of chiral molecules using antennas and nanophotonic metasurfaces[1–9].

Fluorescence intensity is linearly proportional to absorption, so an increase in the local electromagnetic field intensity leads to increased fluorescence intensity. This proportionality forms the basis of fluorescence-detected circular dichroism[10]. Though the signal-to-noise ratio is increased in fluorescence-detected circular dichroism by 1 – 3 orders of magnitude compared to conventional circular dichroism because of increased specificity, the signal is still too low for single-molecule detection[11,12]. Plasmonic antennas like gold nanoparticles (Au NPs) can be used to increase the excitation source photon flux by focusing a continuous plane wave into nanoliter volumes; molecules in that volume therefore absorb more photons. Plasmonic antennas also change the projection of electric fields onto the magnetic fields of the confined wave, and this change in relative temporal and spatial orientation of the light changes the twist of the light. This optical chirality, C, was theorized as a conserved quantity in the late 1960s, and in the last two decades, it has been used to describe differential absorption by chiral molecules[13,14]. Enhancing the optical chirality increases the difference between the absorption of parity-inverted fields, leading to differential absorption of right and left circularly polarized light[15–17].

Near a plasmonic antenna, the fluorescence emission is also modified[18]. The emission from a molecule resonant with a nearby antenna couples with the antenna and the coupled dipole-plasmon mode radiates collectively into the far field[19,20]. However, the emission intensity modification only depends on the position and orientation of the molecule relative to the antenna and is equal for achiral or chiral molecules[21]. Thus, the difference in enhancements in the magnitude of the

fluorescence intensity under left and right circularly polarized light, detected from right-handed molecules near achiral Au NP dimer antennas, is proportional to their differential absorption of the incident field.

In this paper, we measure the fluorescence from single molecules of chiral absorbers—Cy5 J-dimers assembled in double-stranded DNA backbones. The Cy5 J-dimers have been studied under bulk fluorescence, ensemble plasmon-coupled CD measurements, and transient absorption spectroscopy[22–25]. However, while Cy5 has extensively been used in single-molecule localization microscopy, the fluorescence intensity of Cy5 J-dimers is much lower than that of monomeric Cy5 because of the decreased quantum yield (0.039) and increased non-radiative decay rate[26]. Thus, to our knowledge, single Cy5 J-dimers have not been previously detected[27]. We achieved increased detectability of these right-handed molecules near achiral Au NP dimer antennas under right circularly polarized illumination. This strategy offers a new approach to distinguishing weakly fluorescent enantiomers.

Materials and Methods

Au NP dimer antenna substrate

The Au NP dimer (SI Figure S1b) substrate was fabricated on a plasma-cleaned (Yield Engineering Systems, YES-CV200RFS, 180 s in oxygen) glass microscope coverslip (24 × 40 mm, Fisher Scientific 12545D) using electron beam lithography (JEOL JBX-6300FS) as described previously[28]. Briefly, the Au NPs are each 100 nm in length and 60 nm in width and are created by depositing 60 nm Au on a 3-nm thick Ti wetting layer to adhere the NPs to the glass surface. The Au NPs in each dimer are separated by 30 nm, and the Au NP center positions are offset by −50, 0, or +50 nm as described in the text. Adjacent Au NP dimer antennas are separated by 3 μm to avoid lattice resonances. The plasmon resonance of the Au NP dimer antenna has been previously characterized by dark-field scattering spectroscopy to peak at 680 nm[28].

The surface was cleaned using an oxygen plasma etcher (PE-50, Plasma Etch Inc.; 200 mTorr for 25 min), then coated by spin-coating alternating layers of poly(diallyldimethyl-ammonium chloride) (PDADMAC, Sigma-Aldrich, average MW ~200,000 – 350,000, 20 wt% in water) and poly(sodium 4-styrene) (PSS, Sigma-Aldrich, average MW ~ 70,000, 30 wt% in water) to achieve a 6 ± 1 nm PDADMAC-PSS-PDADMAC polymer as detailed previously[29]. The polymer coating

provides an appropriate surface for the adsorption and desorption of dye molecules in single-molecule microscopy and also creates a spacer layer between the Au NP dimer antennas and the dye molecules to minimize fluorescence quenching[29–31]. To avoid cross-contamination, before each subsequent experiment, the Au NP dimer antenna/glass substrate was cleaned using an oxygen plasma etcher to remove the polymer layers and any residual dye, and coated again with the polymer layers.

Electromagnetic simulations of near-field electric field intensity and optical chirality

Full-field electromagnetic simulations of Au NP dimer antennas excited by an incident plane wave were performed with a Finite Domain Time Difference (FDTD) algorithm (Ansys Lumerical FDTD) as described previously[28]. Briefly, the sample geometry was modeled with a fixed mesh with 8 nm^3 voxels near the antennas; an adaptive mesh was used elsewhere. The complex permittivities of Ti and Au were taken from an analytical fit to experimental data[32,33], the glass coverslip was explicitly included (n = 1.5, k = 0), and the Au NP dimers were immersed in water (n = 1.333, k = 0). The total simulation volume was 8 μm^3. The substrate was excited by a plane wave incident along the z-axis from beneath the glass coverslip, and the plane wave excitation was constructed using two plane wave sources with linear polarization along the x- and y-axes with a relative phase of ± 90° to construct right- or left-handed circularly polarized excitation. The electric field, $\boldsymbol{E}$, and magnetic field, $\boldsymbol{B}$, were extracted from a 2D plane monitor placed 6 nm above the coverslip, which is the position of the polymer-water interface at which dye molecules are immobilized for detection. The optical chirality, C, was calculated from $\boldsymbol{E}$ and $\boldsymbol{B}$, as:

$$C = -\frac{\omega}{2c^2} Im\,(E^*.B)$$

where ω is the angular frequency of the radiation, and c is the speed of light. The optical chirality is normalized by the optical chirality of an left circularly polarized plane wave, C_{LCP}, as:

$$C_{LCP} = -\frac{\varepsilon_o\,\omega}{2c^2}\,|E|^2$$

Preparation of chiral DNA-bound Cy5 J-dimers

Two complementary single-stranded DNA oligonucleotides were purchased from Integrated DNA Technologies (iDT): 5′-ACG TCG GTC A Cy5 C GAG AGT GCA-3′ and 5′-TCG AGC CAG T

Cy5 G CTC TCA CGT-3′, each with cyanine 5 (Cy5) inserted at the center of the ssDNA strand. 100 nM stock solutions of the oligonucleotides in IDTE buffer (10 mM trishydroxymethylaminomethane, 0.1 mM ethylenediaminetetraacetic acid) were diluted to 50 nM, and the two complementary oligonucleotide solutions were annealed to form J-dimers of Cy5 held together within a rigid backbone of double-stranded DNA[26] (SI Figure S1a) following the manufacturer's recommended protocol: mix 10 μL of 50 nM solutions, heat at 94 °C for 2 min, and allow to cool to room temperature. When not in use, the annealed DNA was stored at −20 °C.

These Cy5 J-dimers have been previously shown to exhibit high absorption dissymmetry and their 668-nm absorption maximum[26] overlaps with the 680-nm local surface plasmon resonance of the Au NP dimer antenna[25].

Single-molecule fluorescence imaging

A polarimetric epifluorescence microscope system capable of polarization-resolved excitation and sensitive to single-molecule detection was built onto an Olympus IX71 inverted epifluorescence microscope as previously described[28]. Briefly, the 640-nm laser (Coherent CUBE 640-40C) excitation source was cleaned up with a laser excitation filter (Chroma Z640). The excitation linear polarization was controlled with a half-wave plate (Thorlabs AHWP10M-600), a linear polarizer (Thorlabs LPVISB-050-M), and a liquid crystal variable retarder (LCVR, Thorlabs LCC1223T-A) before being focused onto the back focal plane of a 100×, 1.30 numerical aperture (NA) objective (Olympus UPlan FLN) after reflection off a dichroic mirror (Di01-R640). The polarization of the laser was characterized by a linear polarizer (Thorlabs LPVISE100-A) in front of a photodiode above the sample stage. The beam ellipticity, ε, is the square root of the ratio of the minimum power to the maximum power transmitted upon a complete rotation of the linear polarizer, and all experiments were performed with $\varepsilon > 0.95$ [28].

Emission was collected through the same objective in an epifluorescence configuration, and the excitation light was rejected with the same dichroic mirror and an appropriate long-pass filter (Semrock EdgeBasicTM 635 nm). The image was expanded 3× before the image was focused onto a 512 × 512 pixel Andor iXon3 electron-multiplying charge-coupled device camera (1 camera pixel = 53 × 53 nm^2 in the imaging plane).

For imaging, 30 μL of 20 nM Cy5 J-dimer solution was drop-cast onto the Au NP dimer nanoantenna substrate. In this Points Accumulation for Imaging Nanoscale Topography (PAINT) geometry, a sparse subset of Cy5 J-dimers adsorbed onto the surface for single-molecule detection at any one time as described previously[20,34]. A series of 2000-frame fluorescence movies were acquired with an exposure time of 40 ms/frame. The handedness of the incident light was switched between every movie, and to overcome photobleaching, the Cy5 J-dimer dye solution was removed and replenished at the same volume and concentration between every movie. The images were analyzed using the SMALL-LABS algorithm to localize single molecules after subtracting the background signal from the scattering of the Au NP dimer antenna[35]. Molecules emitting at least 800 fluorescence counts/imaging frame were recorded. The localization precision was calculated as the mean of the 95% confidence interval on the Gaussian fits of the localizations.

Results and Discussion

We simulated the excitation of chiral Au NP dimer antennas by plane waves with left or right circularly polarized light. When the handedness of the antenna matches the handedness of the incident polarization, the electric field is strongly enhanced at the antenna center (Figure 1b and SI Figure S2c), and the optical chirality is enhanced in the same region (Figure 1d and SI Figure S2e). Conversely, the electric field enhancement is minimal (Figure 1c and SI Figure S2b), and the optical chirality is close to 0 at the center of the antennas when the handedness of the antenna does not match the incident polarization of the light (Figure 1e and SI Figure S2d). For the achiral Au NP dimer antenna, the electric field enhancement is significant and equal at the antenna center under left and right circularly polarized excitation (Figure 2b-c). The magnitude of optical chirality enhancement is equal, but the handedness of the optical chirality is opposite (Figure 2d-e). We predicted that the differences in electric field and optical chirality profiles near the Au NP dimer antennas would affect the intensity distribution and the probability of detection of the chiral single molecules.

We tested these hypotheses experimentally with single-molecule super-resolution fluorescence imaging of Cy5 J-dimers as they adsorbed transiently on the Au NP dimers from a solution above the Au NP. We set a long (40-ms) imaging integration time such that freely diffusing Cy5 J-dimers were not detected on the EMCCD camera; for every transiently adsorbed Cy5 J-dimers detected, we recorded the fluorescence intensity and apparent position of that single molecule. In this PAINT

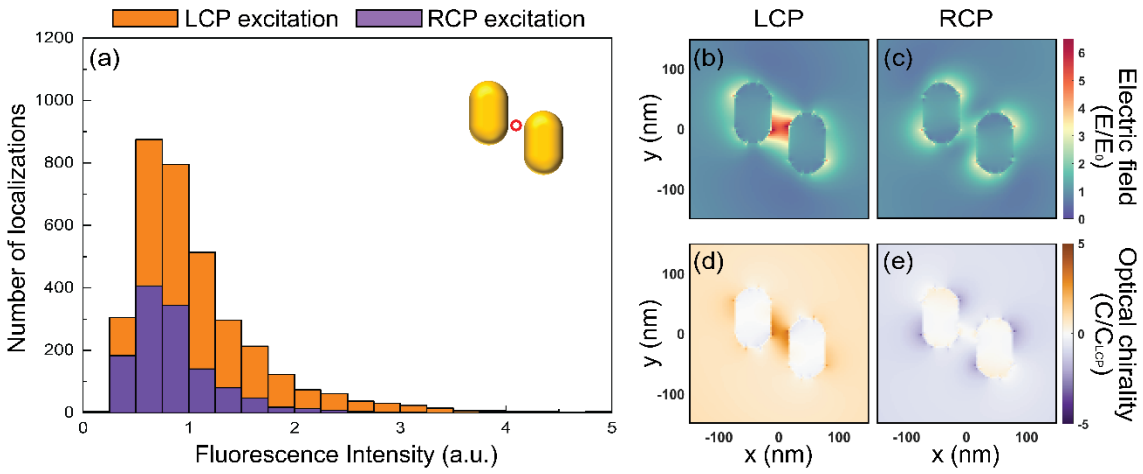

Figure 1. Experimental and computational optical characteristics around left-handed Au NP dimer antennas under left and right circularly polarized light (LCP and RCP, respectively). (a) Distributions of the intensities of molecules detected at the center of the Au NP dimer antenna (apparent position within the red circle; radius = 12.5 nm). (b-e) Profiles in the sample plane calculated from FDTD simulations of Au NP dimer antennas excited by a circularly polarized plane wave incident along the *z*-axis with wavelength 635 nm. (b-c) Electric field enhancement profiles under (b) left and (c) right circularly polarized excitation. (d-e) Optical chirality enhancement profiles under (d) left and (e) right circularly polarized excitation.

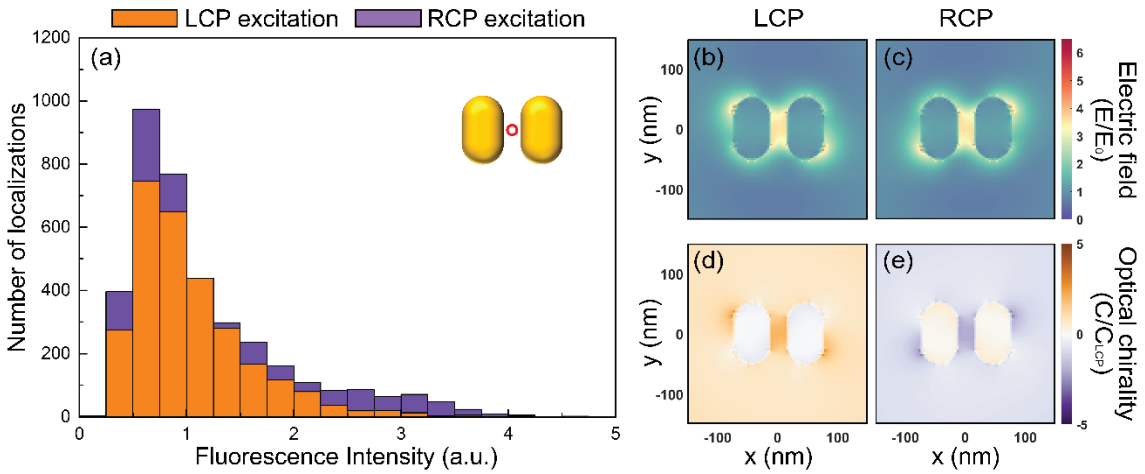

Figure 2. Experimental and computational optical characteristics around achiral Au NP dimer antennas under left and right circularly polarized light (LCP and RCP, respectively). (a) Distributions of the intensities of molecules detected at the center of the Au NP dimer antenna (apparent position within the red circle; radius = 12.5 nm). (b-e) Profiles in the sample plane calculated from FDTD simulations of Au NP dimer antennas excited by a circularly polarized plane wave incident along the *z*-axis with wavelength 635 nm. (b-c) Electric field enhancement profiles under (b) left and (c) right circularly polarized excitation. (d-e) Optical chirality enhancement profiles under (d) left and (e) right circularly polarized excitation.

microscopy configuration, only molecules that are bright enough and immobilized long enough are detected. Fresh Cy5 J-dimer solution was added between movies to overcome photobleaching, and the remaining gradual decrease in the average fluorescence of the molecules was attributed to a gradual increase in photoproducts and photobleached Cy5 J-dimers. We accounted for the difference in intensities by comparing localizations recorded at similar experimental time points: the same amount of time under laser illumination and the same length of time after the addition of fresh Cy5 J-dimer solution.

In each experiment, single Cy5 J-dimers were detected in the vicinity of an array of 25 Au NPs. The detected positions of all single molecules relative to the center of the nearest antenna were compiled. The relative density of localizations was calculated as the number of positions <10 nm away from the molecule position (Figure 3).

In this low signal-to-noise regime, the dimmest molecules are not detected, and the probability of detecting a molecule is related to the number of photons emitted. Since the fluorescence intensity depends on the electric field, molecules adsorbed on the regions with higher electric fields are brighter. As a result, the localization density patterns of chiral single molecules near plasmonic antennas (Figure 3) match the simulated electric field profiles of the near-field electromagnetic field of the particles (Figures 1b-c and 2b-c, and SI Figure S2b-c). The patterns under parity-inverted fields and antennas are also mirror images of each other.

From the localization maps, the single molecules with apparent positions at the center of the antennas can be isolated (Supplementary Note 1) by the average intensity of single Cy5 J-dimers detected at a radius between 450 and 535 nm (SI Figure S1c) from the center of the same antenna during that same movie. We predicted that the Cy5 J-dimers, which are weakly right-handed[26], would be most enhanced when the optical chirality enhancement was the most negative. However, the intensity distributions of the Cy5 J-dimers near Au NP dimer antennas were similar under both handedness of light for all three NP offsets (Figures 1a and 2a; SI Figures S2a and S3). Rather, we measured a significant difference in the number of detected molecules, which is much higher when the incident polarization of light matches the handedness of the Au NP dimer antenna, consistent with the much higher local electric field intensity for these cases (Figure 1b and SI Figure S2c). The electric field enhancement is thus the dominant factor in the increase in the probability of detection; the enhanced optical chirality does not have a significant effect.

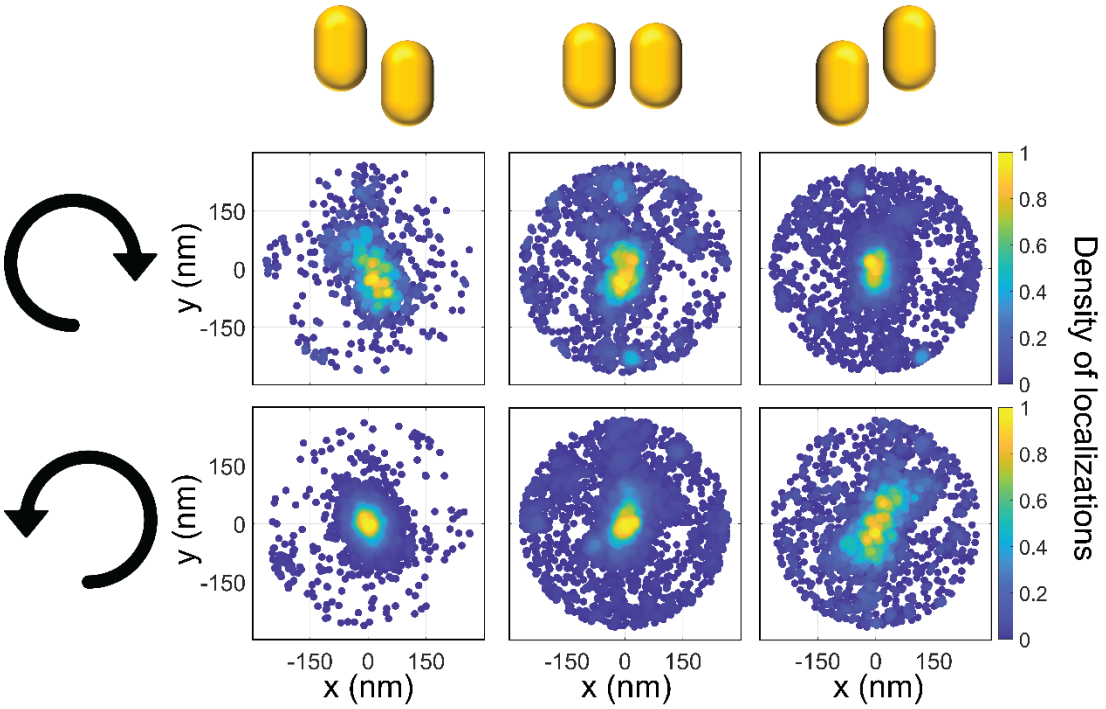

Figure 3. Density of localizations of Cy5 J-dimers detected within 265 nm of a Au NP dimer antenna. Each point is the apparent position of a single detected Cy5 J-dimer relative to the nearest Au NP antenna and the colorscale indicates the number of molecules detected within 10 nm of that position, normalized for each experiment. Excitation wavelength: 635 nm; excitation polarization: right circularly polarized (top) or left circularly polarized light (bottom). The left-handed and right-handed antennas have vertical offsets of ± 50 nm (SI Figure S1). The achiral antenna has no offset. The 95% confidence interval on the fit position is 52 nm with a standard deviation of 19 nm.

Interestingly, for the achiral Au NP dimer antennas, the photon absorption rate and the electric field magnitude are the same in the center region for left and right circularly polarized excitation light (Figure 2b-c). Thus, the increase in the probability of detection of the right-handed J-dimers of Cy5 by 32% under right circularly polarized light near the achiral Au NP dimer antenna (Figure 2a) is attributed to the average increase in fluorescence due to the enhanced optical chirality when the polarization of the excitation light matches the handedness of the Cy5 J-dimer (Figure 2e). This difference in the number of localizations is the only consistent and significant signature of molecular chirality.

Conclusions

Single-molecule localization microscopy of Cy5 J-dimers is challenging due to the uncharacterized fluorescence properties of the probes at the single-molecule level. Here, we achieved this detection and quantified the emission properties of single Cy5 J-dimer molecules by carefully normalizing single-molecule fluorescence intensity measurements to account for experimental artifacts related to non-uniform surface coating and changes in the fluorescence intensities of the molecules over the course of the experiment. We also used circularly polarized incident light to ensure an equal probability of detection for molecules adsorbed along any axis.

The only significant indicator of molecular chirality was the increased detectability of right-handed Cy5 J-dimers near achiral Au NP dimer antennas under right circularly polarized illumination. To further study this detection strategy, future studies should benchmark this measurement based on a pair of chiral probes with similar adsorption rate and quantum yield, but of opposite molecular chirality.

Acknowledgments

This work was supported by National Sciences Foundation grant CHE-1807676 to J.S.B. Thanks to Z. Pfaffenberger for providing the Au NP dimer antenna substrates and to L. McCarthy for helpful conversations about J-dimer preparation.

References

(1) Solomon, M. L.; Abendroth, J. M.; Poulikakos, L. V.; Hu, J.; Dionne, J. A. Fluorescence-Detected Circular Dichroism of a Chiral Molecular Monolayer with Dielectric Metasurfaces. *J. Am. Chem. Soc.* **2020**, *142* (43), 18304–18309. https://doi.org/10.1021/jacs.0c07140.

(2) Solomon, M. L.; Saleh, A. A. E.; Poulikakos, L. V.; Abendroth, J. M.; Tadesse, L. F.; Dionne, J. A. Nanophotonic Platforms for Chiral Sensing and Separation. *Acc. Chem. Res.* **2020**, *53* (3), 588–598. https://doi.org/10.1021/acs.accounts.9b00460.

(3) Mun, J.; Kim, M.; Yang, Y.; Badloe, T.; Ni, J.; Chen, Y.; Qiu, C.-W.; Rho, J. Electromagnetic Chirality: From Fundamentals to Nontraditional Chiroptical Phenomena. *Light Sci. Appl.* **2020**, *9* (1), 139. https://doi.org/10.1038/s41377-020-00367-8.

(4) Warning, L. A.; Miandashti, A. R.; McCarthy, L. A.; Zhang, Q.; Landes, C. F.; Link, S. Nanophotonic Approaches for Chirality Sensing. *ACS Nano* **2021**, *15* (10), 15538–15566. https://doi.org/10.1021/acsnano.1c04992.

(5) Lin, Z.-H.; Zhang, J.; Huang, J.-S. Plasmonic Elliptical Nanoholes for Chiroptical Analysis and Enantioselective Optical Trapping. *Nanoscale* **2021**, *13* (20), 9185–9192. https://doi.org/10.1039/D0NR09080H.

(6) Droulias, S. Chiral Sensing with Achiral Isotropic Metasurfaces. *Phys. Rev. B* **2020**, *102* (7), 075119. https://doi.org/10.1103/PhysRevB.102.075119.

(7) Xu, D.; Lin, Q.; Chang, H.-T. Chiral Ag and Au Nanomaterials Based Optical Approaches for Analytical Applications. *Part. Part. Syst. Charact.* **2019**, *36* (5), 1800552. https://doi.org/10.1002/ppsc.201800552.

(8) Wen, Y.; Li, Z.; Jiang, J. Delving Noble Metal and Semiconductor Nanomaterials into Enantioselective Analysis. *Chin. Chem. Lett.* **2019**, *30* (9), 1565–1574. https://doi.org/10.1016/j.cclet.2019.05.036.

(9) Tang, P.-W.; Tai, C.-Y. Plasmonically Enhanced Enantioselective Nanocolorimetry. *ACS Sens.* **2020**, *5* (3), 637–644. https://doi.org/10.1021/acssensors.9b02037.

(10) Tinoco, I.; Turner, D. H. Fluorescence Detected Circular Dichroism. Theory. *J. Am. Chem. Soc.* **1976**, *98* (21), 6453–6456. https://doi.org/10.1021/ja00437a003.

(11) Prabodh, A.; Wang, Y.; Sinn, S.; Albertini, P.; Spies, C.; Spuling, E.; Yang, L.-P.; Jiang, W.; Bräse, S.; Biedermann, F. Fluorescence Detected Circular Dichroism (FDCD) for Supramolecular Host–Guest Complexes. *Chem. Sci.* **2021**, *12* (27), 9420–9431. https://doi.org/10.1039/D1SC01411K.

(12) Penasa, R.; Begato, F.; Licini, G.; Wurst, K.; Abbate, S.; Longhi, G.; Zonta, C. Fluorescence Detected Circular Dichroism (FDCD) of a Stereodynamic Probe. *Chem. Commun.* **2023**, *59* (44), 6714–6717. https://doi.org/10.1039/D3CC01249B.

(13) Tang, Y.; Cohen, A. E. Optical Chirality and Its Interaction with Matter. *Phys. Rev. Lett.* **2010**, *104* (16), 163901. https://doi.org/10.1103/PhysRevLett.104.163901.

(14) Lipkin, D. M. Existence of a New Conservation Law in Electromagnetic Theory. *J. Math. Phys.* **1964**, *5* (5), 696–700. https://doi.org/10.1063/1.1704165.

(15) Davis, T. J.; Hendry, E. Superchiral Electromagnetic Fields Created by Surface Plasmons in Nonchiral Metallic Nanostructures. *Phys. Rev. B* **2013**, *87* (8), 085405. https://doi.org/10.1103/PhysRevB.87.085405.

(16) Mohammadi, E.; Tavakoli, A.; Dehkhoda, P.; Jahani, Y.; Tsakmakidis, K. L.; Tittl, A.; Altug, H. Accessible Superchiral Near-Fields Driven by Tailored Electric and Magnetic Resonances in All-Dielectric Nanostructures. *ACS Photonics* **2019**, *6* (8), 1939–1946. https://doi.org/10.1021/acsphotonics.8b01767.

(17) Biswas, A.; Cencillo-Abad, P.; Shabbir, M. W.; Karmakar, M.; Chanda, D. Tunable Plasmonic Superchiral Light for Ultrasensitive Detection of Chiral Molecules. *Sci. Adv.* **2024**, *10* (8), eadk2560. https://doi.org/10.1126/sciadv.adk2560.

(18) Mack, D. L.; Cortés, E.; Giannini, V.; Török, P.; Roschuk, T.; Maier, S. A. Decoupling Absorption and Emission Processes in Super-Resolution Localization of Emitters in a Plasmonic Hotspot. *Nat. Commun.* **2017**, *8* (1), 14513. https://doi.org/10.1038/ncomms14513.

(19) Raab, M.; Vietz, C.; Stefani, F. D.; Acuna, G. P.; Tinnefeld, P. Shifting Molecular Localization by Plasmonic Coupling in a Single-Molecule Mirage. *Nat. Commun.* **2017**, *8* (1), 13966. https://doi.org/10.1038/ncomms13966.

(20) Wertz, E.; Isaacoff, B. P.; Flynn, J. D.; Biteen, J. S. Single-Molecule Super-Resolution Microscopy Reveals How Light Couples to a Plasmonic Nanoantenna on the Nanometer Scale. *Nano Lett.* **2015**, *15* (4), 2662–2670. https://doi.org/10.1021/acs.nanolett.5b00319.

(21) Goldwyn, H. J.; Smith, K. C.; Busche, J. A.; Masiello, D. J. Mislocalization in Plasmon-Enhanced Single-Molecule Fluorescence Microscopy as a Dynamical Young's Interferometer. *ACS Photonics* **2018**, *5* (8), 3141–3151. https://doi.org/10.1021/acsphotonics.8b00372.

(22) Slavnova, T. D.; Görner, H.; Chibisov, A. K. Cyanine-Based J-Aggregates as a Chirality-Sensing Supramolecular System. *J. Phys. Chem. B* **2011**, *115* (13), 3379–3384. https://doi.org/10.1021/jp1121118.

(23) Bricks, J. L.; Slominskii, Y. L.; Panas, I. D.; Demchenko, A. P. Fluorescent J-Aggregates of Cyanine Dyes: Basic Research and Applications Review. *Methods Appl. Fluoresc.* **2017**, *6* (1), 012001. https://doi.org/10.1088/2050-6120/aa8d0d.

(24) Lan, X.; Zhou, X.; McCarthy, L. A.; Govorov, A. O.; Liu, Y.; Link, S. DNA-Enabled Chiral Gold Nanoparticle–Chromophore Hybrid Structure with Resonant Plasmon–Exciton Coupling Gives Unusual and Strong Circular Dichroism. *J. Am. Chem. Soc.* **2019**, *141* (49), 19336–19341. https://doi.org/10.1021/jacs.9b08797.

(25) Lin, X.; Zhou, Y.; Pan, X.; Zhang, Q.; Hu, N.; Li, H.; Wang, L.; Xue, Q.; Zhang, W.; Ni, W. Trace Detection of Chiral J-Aggregated Molecules Adsorbed on Single Au Nanorods. *Nanoscale* **2023**, *15* (25), 10667–10676. https://doi.org/10.1039/D3NR01147J.

(26) Markova, L. I.; Malinovskii, V. L.; Patsenker, L. D.; Häner, R. J- vs. H-Type Assembly: Pentamethine Cyanine (Cy5) as a near-IR Chiroptical Reporter. *Chem. Commun.* **2013**, *49* (46), 5298–5300. https://doi.org/10.1039/C3CC42103A.

(27) Eder, T.; Stangl, T.; Gmelch, M.; Remmerssen, K.; Laux, D.; Höger, S.; Lupton, J. M.; Vogelsang, J. Switching between H- and J-Type Electronic Coupling in Single Conjugated

Polymer Aggregates. *Nat. Commun.* **2017**, *8* (1), 1641. https://doi.org/10.1038/s41467-017-01773-0.

(28) Pfaffenberger, Z. J.; Chattopadhyay, S.; Biteen, J. S. Far-Field Polarization Optics Control the Nanometer-Scale Pattern of High-Fluorescence Dissymmetry Emission from Achiral Molecules near Plasmonic Nanodimers. *J. Phys. Chem. C* **2023**, *127* (20), 9663–9672. https://doi.org/10.1021/acs.jpcc.3c00467.

(29) Fu, B.; Flynn, J. D.; Isaacoff, B. P.; Rowland, D. J.; Biteen, J. S. Super-Resolving the Distance-Dependent Plasmon-Enhanced Fluorescence of Single Dye and Fluorescent Protein Molecules. *J. Phys. Chem. C* **2015**, *119* (33), 19350–19358. https://doi.org/10.1021/acs.jpcc.5b05154.

(30) Anger, P.; Bharadwaj, P.; Novotny, L. Enhancement and Quenching of Single-Molecule Fluorescence. *Phys. Rev. Lett.* **2006**, *96* (11), 113002. https://doi.org/10.1103/PhysRevLett.96.113002.

(31) Kulakovich, O.; Strekal, N.; Yaroshevich, A.; Maskevich, S.; Gaponenko, S.; Nabiev, I.; Woggon, U.; Artemyev, M. Enhanced Luminescence of CdSe Quantum Dots on Gold Colloids. *Nano Lett.* **2002**, *2* (12), 1449–1452. https://doi.org/10.1021/nl025819k.

(32) Johnson, P. B.; Christy, R. W. Optical Constants of the Noble Metals. *Phys. Rev. B* **1972**, *6* (12), 4370–4379. https://doi.org/10.1103/PhysRevB.6.4370.

(33) Palik, E. D. *Handbook of Optical Constants of Solids*; Academic Press, 1998.

(34) Sharonov, A.; Hochstrasser, R. M. Wide-Field Subdiffraction Imaging by Accumulated Binding of Diffusing Probes. *Proc. Natl. Acad. Sci.* **2006**, *103* (50), 18911–18916. https://doi.org/10.1073/pnas.0609643104.

(35) Isaacoff, B. P.; Li, Y.; Lee, S. A.; Biteen, J. S. SMALL-LABS: Measuring Single-Molecule Intensity and Position in Obscuring Backgrounds. *Biophys. J.* **2019**, *116* (6), 975–982. https://doi.org/10.1016/j.bpj.2019.02.006.